

pubs.acs.org/journal/ascecg Research Article

# Enhanced N<sub>2</sub> Activation on a Composite Co<sub>3</sub>Mo<sub>3</sub>N Nitride and La<sub>0.6</sub>Sr<sub>0.4</sub>Co<sub>0.2</sub>Fe<sub>0.8</sub>O<sub>3</sub> Perovskite Cathode for High-Temperature Electrochemical Ammonia Synthesis

Matthew Ferree, Seval Gunduz, Jaesung Kim, Raymond LaRosa, Yehia Khalifa, Anne C. Co, and Umit S. Ozkan\*



Cite This: ACS Sustainable Chem. Eng. 2023, 11, 5007–5013



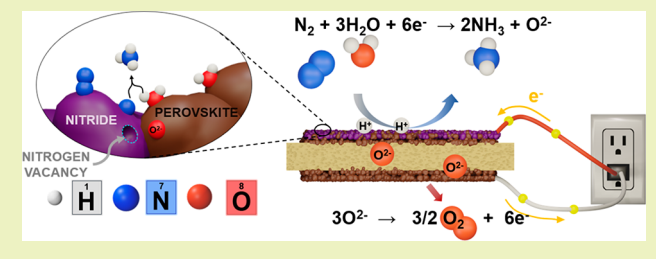
**ACCESS** I

III Metrics & More

Article Recommendations

s Supporting Information

**ABSTRACT:** Electrochemical routes for ammonia synthesis could offer improved conversion efficiency, compatible integration with renewable energy sources, and a solution to distributed chemical production. In a conventional Haber–Bosch process, ammonia,  $NH_3$ , is produced by reacting  $N_2$  and  $H_2$  at high temperatures and pressures. In an electrochemical pathway, the  $H_2$  production and pressurization steps can be bypassed by using  $N_2$  and  $H_2O$  in an ambient-pressure solid-oxide electrolysis cell (SOEC). In this study, a SOEC with a composite cathode of A-site deficient lanthanum



ferrite perovskite oxide and transition metal nitride  $Co_3Mo_3N$  was fabricated, and its activity for the nitrogen reduction reaction (NRR) was studied. The composite cathode produced ammonia at a rate of  $4.0 \times 10^{-11}$  mol s<sup>-1</sup> cm<sup>-2</sup> at 550 °C and 0.65 mA/cm<sup>2</sup>, which was an 8-fold enhancement compared to either of the pure phase electrodes. Relevant properties of  $Co_3Mo_3N$ , such as thermochemical stability, adsorption behavior, and mobility of nitrogen ions, were characterized by various techniques including *in situ* XRD, XAFS/XANES, NAP-XPS, temperature-programmed experiments, and *in situ* DRIFTS.

KEYWORDS: nitrogen fixation, ammonia, electrocatalysis, nitride, SOEC

#### INTRODUCTION

The Haber-Bosch process requires H<sub>2</sub>, typically produced from natural gas, requiring energy-intensive desulfurization to avoid catalyst deactivation, and feed gas pressurization to shift the reaction equilibrium. Electrolysis of N2 and H2O at ambient pressure for ammonia production could greatly improve the sustainability of the ammonia industry by eliminating all these energy intensive steps. Although the field of electrochemical ammonia synthesis by N2 activation is still underdeveloped, there have been a plethora of different types of systems and electrocatalysts considered. Among these studies, most have employed N<sub>2</sub> and H<sub>2</sub> as reactants.<sup>2</sup> Using H<sub>2</sub>O and N<sub>2</sub> brings about more kinetic complexity in the reaction and a greater thermodynamic barrier associated with breaking O-H bonds, but high temperatures (500-600 °C) in a solid oxide electrolysis cell (SOEC) allow for faster reaction kinetics as well as oxide conduction to pull oxygen away from reaction sites. Although developing an active nitrogen reduction reaction (NRR) catalyst for a one-step process using nitrogen and water is highly challenging, the motivation comes from eliminating the hydrogen production and purification steps.

The SOEC half-cell reactions for ammonia synthesis from nitrogen and steam are the following:

Cathode:

$$3H_2O + N_2 + 6e^- \rightarrow 3O^{2-} + 2NH_3$$
 (1)

Anode:

$$3O^{2-} \rightarrow 3/2O_2 + 6e^-$$
 (2)

In this reaction configuration, first attempted by Skodra et al., nitrogen and water react on the cathode surface to form ammonia, and the oxygen evolution reaction (OER) occurs on the anode.<sup>3</sup> Electrical bias drives the flow of oxygen ions toward the anode by reducing H<sub>2</sub>O molecules at the cathode. The hydrogen evolution reaction (HER) from water splitting is the primary competing reaction. HER consumes most of the supplied electrons because the kinetics are much faster than nitrogen reduction, resulting in very low (<1%) Faradaic efficiencies for ammonia production in many cases.<sup>4</sup> Unfortunately, the activation energy requirement for splitting

Received: October 31, 2022 Revised: March 14, 2023 Published: March 21, 2023





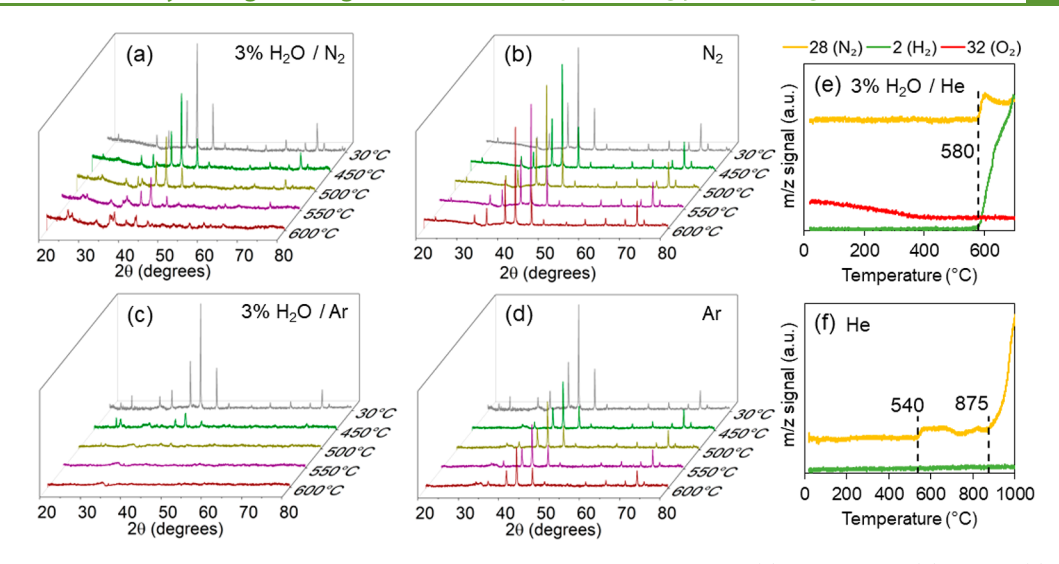


Figure 1. In situ XRD patterns of  $Co_3Mo_3N$  powder heated from room temperature to 600 °C in (a) 3%  $H_2O/N_2$ , (b) dry  $N_2$ , (c) 3%  $H_2O/Ar$ , (d) dry Ar, (e) temperature-programmed reaction of  $Co_3Mo_3N$  powder with 3%  $H_2O/He$  flow, and (f) temperature-programmed decomposition of  $Co_3Mo_3N$  powder with He flow.

the extremely stable dinitrogen bond presents a considerable hurdle in developing selective electrocatalysts.<sup>5</sup>

Perovskite-type oxide materials are common electrodes used in SOECs because of their mixed ionic and electronic conducting (MIEC) properties. They are stable in high temperature environments, and their catalytic properties can be tuned by simply modifying the dopant elements and ratios.<sup>6</sup> A few studies have focused on non-noble metal cathodes for high temperature electrochemical NRR, and some focus on perovskites-based catalysts for the intermediate temperature (300–450 °C) ammonia synthesis. Recently, perovskites have even been studied at ambient conditions for electrochemical nitrogen fixation because oxygen vacancies that form in perovskites are useful for dinitrogen nondissociative anchoring.8 While perovskites have favorable properties for hightemperature electrocatalysis and good activity for H2O electrolysis, new electrodes must be engineered to maximize dinitrogen splitting, which is by far the rate-limiting step in ammonia synthesis. In the present study, we combine the favorable MIEC properties of perovskites with a secondary material—a bimetallic nitride Co<sub>3</sub>Mo<sub>3</sub>N—to boost the nitrogen activation.

It has been shown that nitride (electro)catalysts undergo a Mars-van Krevelen (MvK) mechanism for ammonia synthesis where the lattice nitrogen is protonated to form NH3 and the nitrogen vacancy becomes the active site for N2 adsorption and splitting.<sup>9</sup> Thus, the activated lattice nitrogen becomes an intermediate between N2 and NH3. Transition metal nitride Co<sub>3</sub>Mo<sub>3</sub>N has received particular attention because the nitrogen adsorption energy and turnover frequency of active sites associated with NRR on a Co-Mo bimetallic catalyst appear near the top of the volcano curve next to Ru catalysts. 10 Computational methods confirmed that N-vacancies form appreciably on the Co<sub>3</sub>Mo<sub>3</sub>N surface under traditional ammonia synthesis conditions (400–550  $^{\circ}$ C, pressurized N<sub>2</sub>/  $H_2$ ), but the phenomenon has not been studied using water as the source of protons for NH3 formation. This mechanism is experimentally supported by previous studies where Co<sub>6</sub>Mo<sub>6</sub>N was regenerated to form Co<sub>3</sub>Mo<sub>3</sub>N by exposure to N<sub>2</sub> alone, confirming the existence of replenishable nitrogen vacancies. The present study provides experimental and characterization

data in support of the hypothesis that this favorable MvK mechanism occurs on the nitride surface in the SOEC system during the synthesis of NH<sub>3</sub> from N<sub>2</sub> and H<sub>2</sub>O.

Co<sub>3</sub>Mo<sub>3</sub>N has been studied as an electrocatalyst for ammonia synthesis in two other instances. The first was an intermediate temperature (450 °C) proton-conducting system with the N<sub>2</sub> and H<sub>2</sub> feeds separated by the electrolyte. The second was a K<sup>+</sup> ion pumping system that relies on the electrochemical promotion of catalysis from these alkali metals at the working electrode, where N<sub>2</sub> and H<sub>2</sub> are present. Neither of these studies explored the possibility of using H<sub>2</sub>O for NRR, but our system is capable of H<sub>2</sub>O activation, N<sub>2</sub> splitting, and ionic/electronic conduction due to the composite nitride—perovskite cathode. A composite nitride—perovskite electrode was first demonstrated in our previous publication, and the synergy between these two material types is inspected further in the present study. 14

# ■ RESULTS AND DISCUSSION

Bulk Structural Changes of Co<sub>3</sub>Mo<sub>3</sub>N under High-Temperature Environments. The structure of the ternary nitride Co<sub>3</sub>Mo<sub>3</sub>N powder under various atmospheres up to 600 °C was studied using in situ X-ray diffraction (XRD). The freshly synthesized Co<sub>3</sub>Mo<sub>3</sub>N XRD pattern at room temperature demonstrated a pure crystalline phase. As the powder was heated in 3%  $H_2O/N_2$  (Figure 1a), the crystallinity of the sample decreased, and some impurity phases emerged. The impurities consisted primarily of the bimetallic oxide Co<sub>2</sub>Mo<sub>3</sub>O<sub>8</sub> and the monometallic oxides CoO and MoO<sub>2</sub> (Figure S1), which are a result of the reaction of  $H_2O$  with the sample, replacing the lattice nitrogen with oxygen. Conducting the same procedure in pure nitrogen (Figure 1b) caused negligible changes in the material, confirming the thermal stability of this catalyst. However, this nitride-to-oxide anion substitution by reaction with H<sub>2</sub>O is evidenced by the simultaneous evolution of nitrogen and hydrogen gases observed in the temperature-programmed reaction, shown in Figure 1e, as well as the absence of an O2 peak that is concurrent with the N2 and H2 peaks. This reaction, occurring at 580 °C in Figure 1e, appears to begin at lower temperature in Figure 1a (indicated by oxide impurities), but this is

explained by the dwell and scan time at each temperature for XRD. The crystalline Co<sub>3</sub>Mo<sub>3</sub>N phase remains intact up to 550 °C in the presence of water and nitrogen, but it is no longer detected at 600 °C. Interestingly, the crystal structure deteriorated at a much lower temperature when heated with H<sub>2</sub>O and an inert gas, such as argon (Figure 1c). This indicates that the lattice nitrogen in Co<sub>3</sub>Mo<sub>3</sub>N is mobilized at elevated temperatures and is in equilibrium with the gas phase concentration of nitrogen. Similarly, a slight decrease in crystallinity was observed when the sample was heated in pure argon (Figure 1d), which is contrasted with the apparently perfect stability in the pure nitrogen atmosphere. In light of the structural behaviors observed by in situ XRD and near-ambient pressure XPS (presented below), it is inferred that the surface nitrides decomposed, but the structure below the surface layers remained stable. Temperature-programmed decomposition (Figure 1f) supports this inference with two distinct m/z =28 peaks attributed to the surface and bulk nitrogen, respectively. These surface changes were studied further by XPS, as discussed below.

The changes in the bulk phase of the Co<sub>3</sub>Mo<sub>3</sub>N catalyst were further examined by *ex situ* transmission X-ray absorption fine-structure spectroscopy (XAFS) to elucidate the effect of treatment in humid nitrogen at high temperature. The Co K-edge XANES spectra, shown in Figure 2a, were similar to the

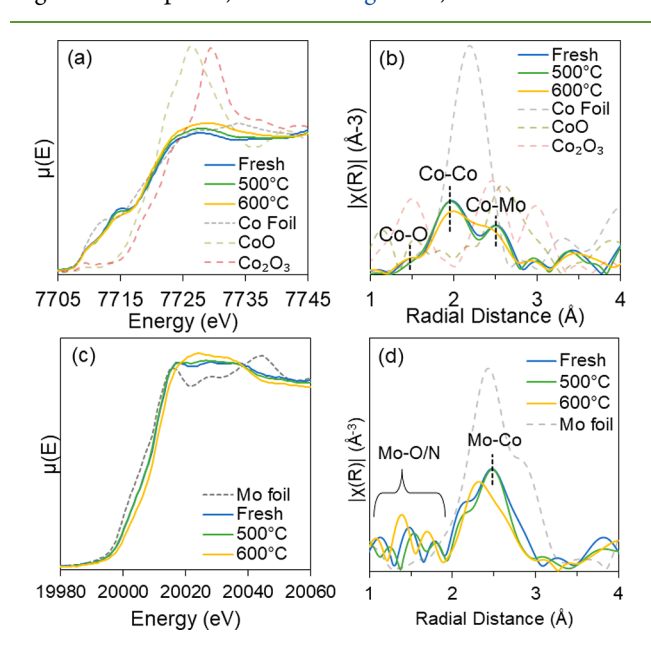


**Figure 2.** Ex situ XANES and XAFS data for (a, b) Co K-edge and (c, d) Mo K-edge spectra of fresh  $Co_3Mo_3N$  powder (blue), powder treated at 500 °C in 3%  $H_2O/N_2$  (green), powder treated at 600 °C in 3%  $H_2O/N_2$  (yellow), and the references foils and oxides (dashed).

Co foil spectrum, exhibiting similar pre- and near-edge features and a weaker white line intensity compared to the oxides. This is expected because the Co atoms are mainly coordinated by other Co atoms in the bimetallic nitride structure and do not bond to the nitrogen. Treating the catalyst with humid nitrogen at 500 and 600 °C weakened the pre-edge features and increased the white line intensity somewhat. This behavior may be attributed to the oxidation of cobalt, but the change is not drastic and the edge shift is within the error range since the spectral resolution was 0.38 eV for this beamline. Plotting the Fourier transform of the XAFS data (Figure 2-b) showed

distinct frequencies corresponding to the Co–O, Co–Co, and Co–Mo interactions in the first (nearest) shell. For the sample that was treated at 600 °C in humid N<sub>2</sub>, the Co–Co and Co–Mo interactions became less distinguishable, forming a broader peak. The Co–Mo peak shifted to a lower frequency and merged with the Co–Co peak, attributed to a change in the coordination of Mo in the structure. <sup>16</sup> The Mo K-edge (Figure 2c) XANES similarly showed an edge shift of  $\sim 1.0$  eV between the fresh and 600 °C treated samples and a shift of the Mo–Co bond length. This suggests a slight positive oxidation state shift for molybdenum atoms, caused by infiltration of oxygen ions. These XAFS frequency distributions suggest the alloying or comingling of Co and Mo by merging the Mo–Co and Mo–Mo peaks into a single broader peak.

Though thermochemical environments cause the catalyst to change or form additional phases like oxides, this can be controlled by the operating temperature and atmosphere. Moreover, the mobility and reactivity of the lattice nitrogen is beneficial for the electrocatalytic activity because active nitride ions are essential for the Mars—van Krevelen type mechanism, which has been shown to occur on such nitride materials, as discussed above. The equilibrium between the lattice and gaseous nitrogen phases—shown by the *in situ* XRD—is evidence that consumed nitrides may be replenished by cleavage of molecular nitrogen during ammonia synthesis.

Surface Electronic Structure Analysis of  $Co_3Mo_3N$ . Ex situ characterization of the freshly prepared catalyst powder by X-ray photoelectron spectroscopy (XPS) was performed to analyze the oxidation states and surface species of the nitride material. In Figure 3a, the Co  $2p_{3/2}$  and  $2p_{1/2}$  orbitals are

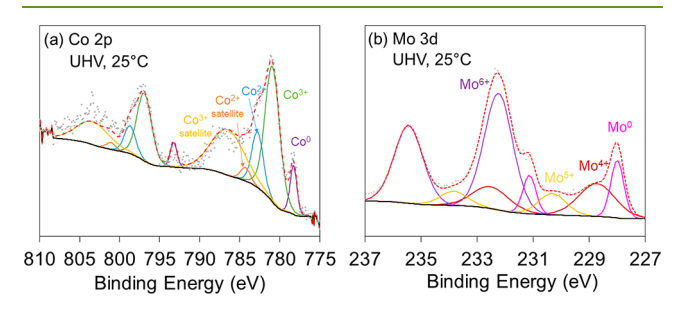


Figure 3. Ex situ XPS spectra for Co<sub>3</sub>Mo<sub>3</sub>N: (a) Co 2p and (b) Mo 3d

shown containing the Co<sup>2+</sup> (782.8 and 798.7 eV) and Co<sup>3+</sup> (780.8 and 796.9 eV) oxidation states. Tatellite peaks are also shown for both oxidation states. The peak at 778.3 eV is assigned to the fully reduced Co<sup>0</sup> oxidation state. In Figure 3b, molybdenum is shown to be present in the Mo<sup>0</sup> (228.0 and 231.1 eV), Mo<sup>4+</sup> (228.7 and 232.5 eV), Mo<sup>5+</sup> (230.3 and 233.8 eV), and Mo<sup>6+</sup> (232.2 and 235.4 eV) oxidation states. <sup>18</sup> The prominence of higher Mo oxidation states is not surprising since each Mo atom in the structure is coordinated with two N atoms, which strongly pull electrons away from Mo. The Mo<sup>0</sup> oxidation state is explained by the bonds to other Mo and Co atoms, which have very similar electronegativities. The N 1s region in Figure S2a largely overlaps with the Mo 3p<sub>3/2</sub> region. However, a strong N 1s peak at 397.9 eV indicates bonding of nitrogen to metal ions in the surface structure. Oxygen bonds are also evidenced in the O 1s region shown in Figure S2b. After ammonolysis, the catalyst was exposed to air at room temperature. This caused some metal-oxygen bonds to form

on the surface, which corresponds to the peak at 530.5 eV. The peak at 531.5 eV is ascribed to hydroxyls or adsorbed moisture.

The behavior of the catalyst surface structure under high-temperature conditions was analyzed by NAP-XPS (Figure 4).

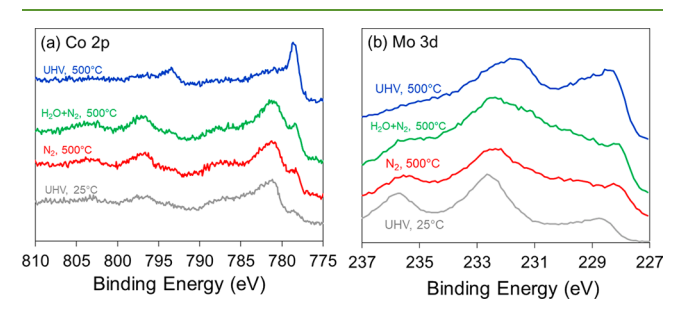


Figure 4. NAP-XPS spectra for  $Co_3Mo_3N$  at room temperature in a vacuum and at 500 °C under 2 mbar  $N_2$ , 1 mbar  $H_2O$  + 1 mbar  $N_2$ , and a vacuum: (a) Co 2p and (b) Mo 3d.

When the Co<sub>3</sub>Mo<sub>3</sub>N powder was heated to 500 °C under 1 Torr N<sub>2</sub>, the Co 2p and Mo 3d spectra remained the same as the pretreatment room temperature scans. Subsequent exposure to H2O slightly decreased the concentration of higher oxidation states in the Mo 3d spectrum and shifted the distribution of the Co 2p region to a slightly more positive oxidation state, which demonstrates that the surface interacts with the H<sub>2</sub>O/N<sub>2</sub> atmosphere without entirely oxidizing/ decomposing. However, when the fresh Co<sub>3</sub>Mo<sub>3</sub>N was heated to 500 °C under ultrahigh vacuum (~10-8 Torr), the concentrations of both zerovalent Co<sup>0</sup> and Mo<sup>0</sup> significantly increased, and the higher oxidation states almost entirely disappeared. Since there is no gaseous N<sub>2</sub> to stabilize the lattice-gas phase equilibrium, as discussed above, the mobilized nitrogen ions combine to form gaseous N2, which was detected by the residual gas analyzer. This may have created a Co<sub>6</sub>Mo<sub>6</sub>N, bimetallic alloy, or another nitrogendeficient phase on the surface.

Adsorption Behavior on  $\text{Co}_3\text{Mo}_3\text{N}$  and LSCF Catalysts. The interaction of the catalyst surfaces with reactants was studied by *in situ* diffuse reflectance infrared Fourier transform spectroscopy (DRIFTS) experiments. The surfaces of  $\text{Co}_3\text{Mo}_3\text{N}$  and LSCF were compared by a time-dependent adsorption/desorption study to show the interactions of  $\text{H}_2\text{O}$  and  $\text{N}_2$  at the gas—solid interface. The formation of N—H species on the catalyst surfaces from exposure to humid nitrogen is of particular interest. The catalyst was pretreated in dry nitrogen up to 450 °C to remove excess adsorbent species from the air. When the catalyst was exposed to humid nitrogen  $(3\% \text{ H}_2\text{O}/\text{N}_2)$  at t=0 min, scans every 5 min at 400 °C revealed the gradual formation of N—H species.

In Figure 5, the flat line labeled as "0 min, N<sub>2</sub>" is the initial condition at 400 °C with no peaks because the initial scan and the background were both taken under the dry nitrogen condition after pretreatment. However, once the humidity was introduced, peaks began to appear on the Co<sub>3</sub>Mo<sub>3</sub>N scans between 3200–2800 cm<sup>-1</sup>, which are attributed to N–H stretching, but there was no evidence of N–H adsorbents on the LSCF in this wavelength range. The feed was switched back to dry nitrogen, and scans were taken for an additional 30 min (data not shown), but these peaks did not disappear, indicating strong adsorption energy. Any moisture or OH species have desorbed well below 400 °C, evidenced by the absence of a broad peak between 3700–2700 cm<sup>-1</sup> and sharp

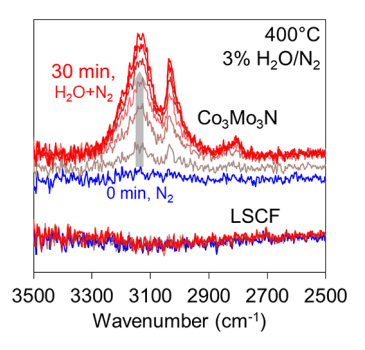
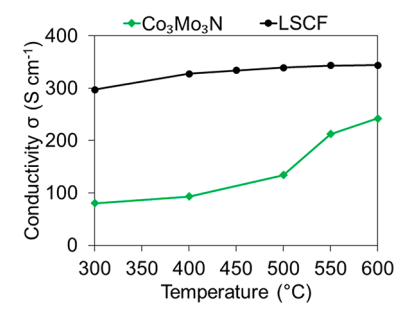


Figure 5. DRIFT spectra of  $Co_3Mo_3N$  and LSCF surfaces at 400  $^{\circ}C$  as a function of time over 30 min of exposure to humidity.

peak at  $1600~\rm cm^{-1}$ , as shown in the lower temperature experiment in Figure S3a,b. Peaks similar to those in Figure 5 were observed by *in situ* DRIFTS reduction experiments performed on these catalysts using 5%  $\rm H_2/N_2$  atmosphere (Figure S3c), confirming the identification of these peaks. At  $150~\rm ^{\circ}C$ , the rates of  $\rm H_2O$  adsorption/desorption for  $\rm Co_3Mo_3N$  and LSCF appear to be indistinguishable, which means these catalysts have similar  $\rm H_2O$  affinity. However, the striking difference in behavior for the N–H formation on the two catalysts indicates that  $\rm Co_3Mo_3N$  possesses enhanced ability to reduce nitrogen.

**Electrochemical Performance.** Electrical conductivity of  $Co_3Mo_3N$  and LSCF catalysts was measured under dry  $N_2$  between 300 and 600 °C. As shown in Figure 6, LSCF



**Figure 6.** Electrical conductivity measurements of catalyst pellets by DC 4-point probe method in N<sub>2</sub> atmosphere.

possesses a higher conductivity. The conductivity of the nitride is moderately high due to its  $\eta$ -carbide structure and increases significantly above 500 °C. It is rationalized that the conductivity increases within the temperature range where the anions become mobilized. <sup>19</sup>

The electrocatalytic activity experiments were performed under  $3\%~H_2O/N_2$  atmosphere within the temperature range of  $500-600~^{\circ}C$  and  $0.25-3~^{\circ}M$  applied bias. The button cells were fabricated and tested as described in the Experimental Methods. An initial screening experiment (Figure S4a) was performed to optimize the temperature and applied bias for the production rate of ammonia. With respect to applied bias, the NH $_3$  production followed a volcano-shaped curve with a maximum at 1 mA, which is attributed to the competing hydrogen evolution reaction and OH species saturating the catalyst active sites at higher currents. The optimum temperature appears to be around 550  $^{\circ}C$ , which is consistent with the *in situ* XRD and XAFS data because the nitride ions are mobilized—yet not too unstable—at this temperature. A stability test (Figure S4b) was also conducted to confirm that

catalyst degradation, product inhibition, or other time-dependent nuisance variables were not confounding the data. If the production of ammonia were merely a byproduct of hydrolyzing the nitride, we would expect the production rate to decrease over time. However, the ability of this electrocatalyst to replenish nitrogen ions from N<sub>2</sub>, as investigated by *in situ* XRD and NAP-XPS, allows for an apparent steady-state between the consumption and replenishment of nitrogen in the structure

In Figure 7, the composite cathode performed significantly better than either the pure perovskite cathode or the pure

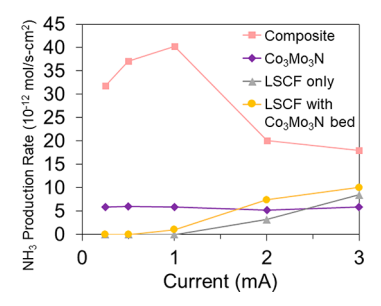


**Figure 7.** Ammonia synthesis activity under 3%  $H_2O/N_2$  at 550  $^{\circ}C$  and 0.25-3 mA. Production rates averaged over 1 h of reaction time for each data point.

nitride, indicating some synergy between the two materials in electrochemical NH3 production. As hypothesized, these two materials work together because the LSCF has favorable electronic/ionic conductive properties and activates H2O, but the Co<sub>3</sub>Mo<sub>3</sub>N interacts readily with gaseous N<sub>2</sub>, which is essential for this reaction. These concepts are also consistent with the trends observed in the pure phase electrodes. The production rate of NH<sub>3</sub> on the Co<sub>3</sub>Mo<sub>3</sub>N electrode appears to be independent of applied potential because O<sup>2-</sup> ions from H<sub>2</sub>O splitting cannot be easily produced or transported away from reaction sites. Also, the NH<sub>3</sub> production rate on the LSCF cathode is low but displays a positive trend with respect to applied bias. LSCF is known to be an active and efficient electrocatalyst for H2O electrolysis, so a pure LSCF cathode would readily produce hydrogen which may react with N<sub>2</sub> to produce a small amount of NH3 through the Haber-Bosch reaction. This observation also serves as some evidence that the NH<sub>3</sub> detected from the composite cathode is not primarily a result of a gas phase reaction between H2 and N2. Many of these conditions were repeated on either the same cell or a different cell under identical conditions to confirm the quantitative reproducibility of these results and the trends with respect to temperature and electrical bias.

The electrochemical nature of the NH $_3$  formation enhancement was further confirmed by adding a catalyst bed of Co $_3$ Mo $_3$ N to the reaction chamber with a pure LSCF electrode. The catalyst bed was supported by glass wool and set up such that it was physically and electrically separated from the cathode, but the effluent made sufficient contact with the Co $_3$ Mo $_3$ N catalyst at 550 °C (see Figure SS). This tested the possibility that NH $_3$  formation may be occurring primarily by electrochemical hydrogen production and subsequent nonelectrocatalytic reaction of the produced H $_2$  with N $_2$ . In this setup, where the nitride and perovskite oxide phases were not in electrical contact, the NH $_3$  formation rates were much lower than the composite cathode and very similar to the LSCF cathode only. This experiment showed that the

 $Co_3Mo_3N$  must be part of the cathode to electrocatalytically activate  $N_2$  for  $NH_3$  formation, ruling out the possibility that the ammonia formation observed is due to the catalytic Haber–Bosch reaction. Although  $Co_3Mo_3N$  has been shown to catalyze ammonia formation from  $N_2$  and  $H_2$ , this reaction is negligible compared to the electrocatalytic process.<sup>20</sup>

#### CONCLUSIONS

The evidence presented in this study for lattice-gas phase nitrogen equilibrium and for nitrogen reduction occurring on the nitride surface signifies that Co<sub>3</sub>Mo<sub>3</sub>N activates N<sub>2</sub> more readily than the perovskite oxide. The equilibrium between the nitride anions and N2 is supported by in situ XRD and NAP-XPS, which revealed that the crystal structure is stabilized by the presence of N<sub>2</sub>. The mobility/reactivity of the lattice N is shown by XAFS, NAP-XPS, and temperature-programmed reaction. The ability of the Co<sub>2</sub>Mo<sub>3</sub>N to form N-H bonds was studied by in situ DRIFTS. Electrochemical activity testing confirmed that the composite Co<sub>3</sub>Mo<sub>3</sub>N-LSCF electrode was superior to either of the pure phase electrodes due to the synergy between the nitrogen activation ability of Co<sub>3</sub>Mo<sub>3</sub>N and the MIEC properties of LSCF, though the precise reaction mechanism would require further study. Ammonia was electrochemically produced from 3% H<sub>2</sub>O/N<sub>2</sub> on the button cell cathode with a formation rate of  $4.0 \times 10^{-11}$  mol s<sup>-1</sup> cm<sup>-2</sup> at 550 °C and 0.65 mA/cm<sup>2</sup>.

#### EXPERIMENTAL METHODS

Catalyst Synthesis. The  $Co_3Mo_3N$  catalyst was synthesized by nitridation of the  $CoMoO_4$  precursor, while the precursor was obtained by coprecipitation. The synthesis procedure is based on literature. Starting with ammonium polymolybdate ( $(NH_4)_6Mo_7O_{24}\cdot 4H_2O$ ) dissolved in deionized water at 50 °C, the pH was adjusted to 6.0 using ammonium hydroxide solution. Cobalt nitrate ( $Co(NO_3)_2\cdot 6H_2O$ ) was dissolved separately in the same volume of water as the molybdenum solution and added dropwise under constant agitation to the molybdenum solution. Once combined, the solution was further heated to 90 °C and stirred for 1 h. Vacuum filtration was performed to obtain a purple precipitate, which was washed twice with deionized water and once with ethanol. The precipitate was dried at 120 °C. Calcination in air at 550 °C for 2 h formed the  $CoMoO_4$  structure.

Nitridation of the  $CoMoO_4$  precursor was accomplished by ammonolysis. The tube furnace was first purged with nitrogen at room temperature for 1 h. The sample was slowly heated, switching to pure  $NH_3$  feed at 350 °C and holding for 5 h at 785 °C. Gas flow was switched back to nitrogen when the furnace cooled to below 350 °C. Air was slowly injected back into the system to passivate the catalyst before removing the sample at room temperature.

**Characterization of Co<sub>3</sub>Mo<sub>3</sub>N.** *In situ* X-ray diffraction (XRD) was performed in a Bruker D8 powder X-ray diffractometer with an Anton Paar HTK1200 oven attachment to control the temperature and gaseous environment. The bulk crystalline structure of  $Co_3Mo_3N$  was analyzed at temperatures from 30 to 600 °C with mixtures of  $N_2$ , Ar, and/or  $H_2O$  vapor. The X-ray source is a Cu K $\alpha$  source, and the generator operates at 40 kV and 40 mA. Scans were performed within the 20° to 80°  $2\theta$  range, and the step size was 0.019° per 0.5 s. A water bubbler at 20 °C and 1 atm was used to deliver wet nitrogen and argon feed gases. The sample was held at each temperature for 15 min before the scan commenced.

Temperature-programmed decomposition and reaction experiments were performed on a bed of  $\mathrm{Co_3Mo_3N}$  catalyst powder in a controlled atmosphere. Samples were prepared by packing a quartz reactor tube (4.0 mm ID) with 50 mg of catalyst powder, held in place by glass wool. The quartz tube was placed inside a small vertical tube furnace. The gas mixture was flowed through the catalyst bed, and a

portion of the effluent was sent to an MKS Cirrus mass spectrometer. A linear temperature ramp was applied to the catalyst bed while the mass spectrometer continuously monitored the effluent.

X-ray photoelectron spectroscopy (XPS) was conducted using a Kratos Axis Ultra XPS instrument for ex situ analysis. The Kratos XPS instrument uses a monochromated Al K $\alpha$  X-ray source (1486 eV, 12 kV, 10 mA) and an ultrahigh vacuum (~10<sup>-9</sup> Torr) chamber. Nearambient pressure XPS (NAP-XPS) was conducted on the catalyst powder to analyze the changes in surface character under reaction-like environments. These experiments were performed at the Ohio State University's Surface Analysis Laboratory using a SPECS NAP-XPS system equipped with a monochromated Al K $\alpha$  X-ray source (1486) eV). The analyzer is a 1-D DLD SPECS PHOIBOS NAP analyzer capable of 1 meV resolution. The catalyst was deposited on a 9 mm × 9 mm rectangular YSZ substrate and loaded into the ultrahigh vacuum (UHV) chamber at room temperature. Nitrogen gas (99.999% purity) and water vapor (introduced via a bulb containing MilliO water which was freeze pump thawed three times) were fed to the chamber to reach a total chamber pressure of 2 mbar using mass flow controllers. The sample was heated by conduction from the uncoated side of the substrate until the catalyst surface reached 773 K (500 °C). High resolution spectra were collected for Co 2p, Mo 3d, O 1s, and N 1s, as well as a survey scan.

The in situ DRIFTS technique was used to observe the adsorption/desorption behavior on the catalyst surfaces at elevated temperature. The adsorption of  $\rm H_2O$  and  $\rm N_2$  on the  $\rm Co_3Mo_3N$  and LSCF catalysts was observed using a Thermoelectron Nicolet 6700 FTIR equipped with an MCT detector. The catalysts were diluted with potassium bromide in a 1:20 mass ratio of catalyst to KBr, and the samples were pretreated at 450 °C under  $\rm N_2$ . The temperature was decreased to the desired temperature and held constant. Scans were taken in the wavelength range of 4000–1300 cm $^{-1}$  every 5 min after switching to the  $\rm H_2O/N_2$  environment for the 30 min adsorption phase. Scans continued every 5 min after switching back to dry  $\rm N_2$  for the 30 min desorption phase.

Three samples were prepared for *ex situ* X-ray absorption fine structure spectroscopy (XAFS). The samples included freshly synthesized  ${\rm Co_3Mo_3N}$  and  ${\rm Co_3Mo_3N}$  after treatment in 3%  ${\rm H_2O/N_2}$  at 500 and 600 °C for 2 h. The XAFS experiments were conducted at the Sector 10-ID of MRCAT (Materials Research Collaborative Access Team) division at Argonne National Laboratory. The powdered samples were smeared on a piece of Scotch tape and folded into multiple layers to obtain one adsorption length at X-ray energies of 7709 eV (Co K-edge) and 20000 eV (Mo K-edge). The XAFS measurements on the  ${\rm Co_3Mo_3N}$  samples were done in transmission mode, and each measurement on the samples was coupled with X-ray absorption spectra of the corresponding metal foil to calibrate the data for any shift in X-ray energy.

**Electrocatalytic Activity Measurement.** The button cells used in the activity experiments were fabricated using commercial yttria-stabilized zirconia (YSZ) electrolyte substrates, gadolinium-doped ceria (GDC) powder, and (La<sub>0.6</sub>Sr<sub>0.4</sub>)<sub>0.95</sub>Co<sub>0.2</sub>Fe<sub>0.8</sub>O<sub>3</sub> (LSCF) catalyst powder from Nextech Materials. A GDC interlayer was screen-printed on both sides of the YSZ electrolyte and fired in nitrogen at 1400 °C for 2 h. LSCF was then screen-printed on both sides with an electrode area of 1.53 cm² covering the GDC layer and sintered in air at 1200 °C for 5 h. Silver wire was attached to the electrodes using high-temperature conductive silver paste, and then one side was coated with a 7:3 Co<sub>3</sub>Mo<sub>3</sub>N:LSCF mixture by spray deposition. Button cells with pure Co<sub>3</sub>Mo<sub>3</sub>N and pure LSCF cathodes were also fabricated for comparison.

The prepared button cells were placed on top of an alumina tube and sealed using Aremco seal 611. The silver wires were connected to a Keithley 6220 current source and Keithley 6182 nanovoltmeter for current application and voltage measurement, respectively. A stream of wet nitrogen  $(3\%~H_2O/N_2)$  was supplied to the cathode side. The reactor effluent was bubbled through an aqueous solution of 0.01 M HCl to capture the ammonia product. The applied cell current was tested in the range of 0.15–2 mA/cm² and at 500–600 °C. The dissolved ammonia was quantified after 1 h of reaction time by the

Nessler's reagent method using Hanna Instruments Ammonia Low Range Photometer HI96700C, which has a resolution and lower detection limit of 1 ppm of NH<sub>3</sub>. Note that the initial screening experiment used shorter reaction durations and the gas-sensing electrode method Thermo Scientific Orion 9512 Ammonia Electrode connected to an Orion Dual Star pH/ISE meter.

#### ASSOCIATED CONTENT

## **Solution** Supporting Information

The Supporting Information is available free of charge at https://pubs.acs.org/doi/10.1021/acssuschemeng.2c06520.

Additional characterization and performance data for the  $Co_3Mo_3N$  catalyst (PDF)

## AUTHOR INFORMATION

#### **Corresponding Author**

Umit S. Ozkan — William G. Lowrie Department of Chemical and Biomolecular Engineering, The Ohio State University, Columbus, Ohio 43210, United States; ⊙ orcid.org/0000-0001-5571-2257; Email: ozkan.1@osu.edu

#### **Authors**

Matthew Ferree – William G. Lowrie Department of Chemical and Biomolecular Engineering, The Ohio State University, Columbus, Ohio 43210, United States

Seval Gunduz – William G. Lowrie Department of Chemical and Biomolecular Engineering, The Ohio State University, Columbus, Ohio 43210, United States

Jaesung Kim – William G. Lowrie Department of Chemical and Biomolecular Engineering, The Ohio State University, Columbus, Ohio 43210, United States

Raymond LaRosa – William G. Lowrie Department of Chemical and Biomolecular Engineering, The Ohio State University, Columbus, Ohio 43210, United States

Yehia Khalifa — Department of Chemistry and Biochemistry, The Ohio State University, Columbus, Ohio 43210, United States

Anne C. Co − Department of Chemistry and Biochemistry, The Ohio State University, Columbus, Ohio 43210, United States; © orcid.org/0000-0002-3546-1582

Complete contact information is available at: https://pubs.acs.org/10.1021/acssuschemeng.2c06520

#### **Author Contributions**

Matthew Ferree: conceptualization, investigation, methodology, data curation, formal analysis, writing—original draft. Seval Gunduz: investigation, formal analysis, writing review and editing. Jaesung Kim: investigation, formal analysis, writing—review and editing. Raymond LaRosa: materials synthesis, data collection, writing—review and editing. Yehia Khalifa: XPS characterization, formal analysis, writing—review. Anne C. Co: formal analysis, writing—review. Umit S. Ozkan: conceptualization, funding acquisition, project administration, resources, supervision, formal analysis, writing—review and editing.

#### Notes

The authors declare no competing financial interest.

#### ACKNOWLEDGMENTS

We would like to gratefully acknowledge the financial support provided for this work by the U.S. National Science Foundation (Chemical, Bioengineering, Environmental, and Transport Systems-CBET Division), under Award Number 1932638, and the U.S. Department of Energy (Office of Science, Office of Basic Energy Sciences), under the Award Number DE-FG02-07ER15896. This research used resources of the Advanced Photon Source, a U.S. Department of Energy (DOE) Office of Science User Facility, operated for the DOE Office of Science by Argonne National Laboratory under Contract No. DE-AC02-06CH11357. X-ray photoelectron spectroscopy was performed at the Surface Analysis Laboratory at the Ohio State University.

#### ABBREVIATIONS

SOEC, solid oxide electrolysis cell; NRR, nitrogen reduction reaction; XRD, X-ray diffraction; XAFS, X-ray absorption fine-structure spectroscopy; XANES, X-ray absorption near edge spectroscopy; NAP-XPS, near-ambient pressure X-ray photo-electron spectroscopy; DRIFTS, diffuse reflectance infrared Fourier transform spectroscopy; HER, hydrogen evolution reaction; MIEC, mixed ionic—electronic conductor; MvK, Mars—van Krevelen; LSCF, lanthanum strontium cobalt ferrite perovskite; YSZ, yttria-stabilized zirconia; GDC, gadolinium-doped ceria

## REFERENCES

- (1) Gunduz, S.; Deka, D. J.; Ozkan, U. S. A review of the current trends in high-temperature electrocatalytic ammonia production using solid electrolytes. *J. Catal.* **2020**, *387*, 207–216.
- (2) Kyriakou, V.; Garagounis, I.; Vasileiou, E.; Vourros, A.; Stoukides, M. Progress in the electrochemical synthesis of ammonia. *Catal. Today* **2017**, 286, 2–13.
- (3) Skodra, A.; Stoukides, M. Electrocatalytic synthesis of ammonia from steam and nitrogen at atmospheric pressure. *Solid State Ionics* **2009**, *180* (23–25), 1332–1336.
- (4) Xu, H.; Ithisuphalap, K.; Li, Y.; Mukherjee, S.; Lattimer, J.; Soloveichik, G.; Wu, G. Electrochemical ammonia synthesis through N2 and H2O under ambient conditions: Theory, practices, and challenges for catalysts and electrolytes. *Nano Energy* **2020**, *69*, 104469.
- (5) Van der Ham, C. J.; Koper, M. T.; Hetterscheid, D. G. Challenges in reduction of dinitrogen by proton and electron transfer. *Chem. Soc. Rev.* **2014**, *43* (15), 5183–5191.
- (6) Deka, D. J.; Gunduz, S.; Fitzgerald, T.; Miller, J. T.; Co, A. C.; Ozkan, U. S. Production of syngas with controllable H2/CO ratio by high temperature co-electrolysis of CO2 and H2O over Ni and Codoped lanthanum strontium ferrite perovskite cathodes. *Applied Catalysis B: Environmental* **2019**, 248, 487–503.
- (7) Zhang, M.; Jeerh, G.; Zou, P.; Lan, R.; Wang, M.; Wang, H.; Tao, S. Recent development of perovskite oxide-based electrocatalysts and their applications in low to intermediate temperature electrochemical devices. *Mater. Today* **2021**, *49*, 351–377.
- (8) Zhang, S.; Duan, G.; Qiao, L.; Tang, Y.; Chen, Y.; Sun, Y.; Wan, P.; Zhang, S. Electrochemical ammonia synthesis from N2 and H2O catalyzed by doped LaFeO3 perovskite under mild conditions. *Ind. Eng. Chem. Res.* **2019**, 58 (20), 8935–8939.
- (9) Zeinalipour-Yazdi, C. D.; Hargreaves, J. S.; Catlow, C. R. A. Nitrogen activation in a Mars—van Krevelen mechanism for ammonia synthesis on Co3Mo3N. *J. Phys. Chem. C* **2015**, *119* (51), 28368—28376.
- (10) Jacobsen, C. J.; Dahl, S.; Clausen, B. S.; Bahn, S.; Logadottir, A.; Nørskov, J. K. Catalyst design by interpolation in the periodic table: bimetallic ammonia synthesis catalysts. *J. Am. Chem. Soc.* **2001**, 123 (34), 8404–8405.
- (11) Gregory, D.; Hargreaves, J.; Hunter, S. On the Regeneration of Co3Mo3N from Co6Mo6N with N2. *Catal. Lett.* **2011**, 141 (1), 22–26.

- (12) Amar, I. A.; Lan, R.; Petit, C. T.; Tao, S. Electrochemical Synthesis of Ammonia Based on Co 3 Mo 3 N Catalyst and LiAlO 2—(Li, Na, K) 2 CO 3 Composite Electrolyte. *Electrocatalysis* **2015**, 6 (3), 286–294.
- (13) Díez-Ramírez, J.; Kyriakou, V.; Garagounis, I.; Vourros, A.; Vasileiou, E.; Sánchez, P.; Dorado, F.; Stoukides, M. Enhancement of ammonia synthesis on a Co3Mo3N-Ag electrocatalyst in a K- $\beta$ Al2O3 solid electrolyte cell. ACS Sustainable Chem. Eng. 2017, 5 (10), 8844–8851
- (14) Gunduz, S.; Deka, D. J.; Ferree, M.; Kim, J.; Millet, J.-M. M.; Ozkan, U. S.; Co, A. C. Composite Cathodes with Oxide and Nitride Phases for High-Temperature Electrocatalytic Ammonia Production from Nitrogen and Water. *ECS Advances* **2022**, *1* (1), 014501.
- (15) Co<sub>3</sub>Mo<sub>3</sub>N (Mo<sub>3</sub>Co<sub>3</sub>N) Crystal Structure: Datasheet from "PAULING FILE Multinaries Edition 2012" in Springer Materials); Springer-Verlag Berlin Heidelberg & Material Phases Data System (MPDS), Switzerland & National Institute for Materials Science (NIMS), Japan. https://materials.springer.com/isp/crystallographic/docs/sd\_1612015 (accessed 10-04-2022).
- (16) Feng, K.; Tian, J.; Zhang, J.; Li, Z.; Chen, Y.; Luo, K. H.; Yang, B.; Yan, B. Dual Functionalized Interstitial N Atoms in Co3Mo3N Enabling CO2 Activation. ACS Catal. 2022, 12 (8), 4696–4706.
- (17) Chu, H.; Zhang, D.; Jin, B.; Yang, M. Impact of morphology on the oxygen evolution reaction of 3D hollow Cobalt-Molybdenum Nitride. *Applied Catalysis B: Environmental* **2019**, 255, 117744.
- (18) Podila, S.; Zaman, S. F.; Driss, H.; Al-Zahrani, A. A.; Daous, M. A.; Petrov, L. A. High performance of bulk Mo2N and Co3Mo3N catalysts for hydrogen production from ammonia: Role of citric acid to Mo molar ratio in preparation of high surface area nitride catalysts. *Int. J. Hydrogen Energy* **2017**, *42* (12), 8006–8020.
- (19) Prior, T. J.; Battle, P. D. Superparamagnetism and metal-site ordering in quaternary nitrides with the  $\eta$ -carbide structure. *J. Mater. Chem.* **2004**, *14* (20), 3001–3007.
- (20) Zeinalipour-Yazdi, C. D.; Hargreaves, J. S.; Catlow, C. R. A. DFT-D3 study of molecular N2 and H2 activation on Co3Mo3N surfaces. *J. Phys. Chem. C* **2016**, *120* (38), 21390–21398.
- (21) Mckay, D.; Hargreaves, J.; Rico, J.; Rivera, J.; Sun, X.-L. The influence of phase and morphology of molybdenum nitrides on ammonia synthesis activity and reduction characteristics. *J. Solid State Chem.* **2008**, *181* (2), 325–333.